JOC The Journal of Organic Chemistry

pubs.acs.org/joc Article

Unusual Acetonitrile Adduct Formed via Photolysis of 4′-Chloro-2-Hydroxybiphenyl in Aqueous Solution

Xiting Zhang, Yan Guo, Erin Dallin, Jiani Ma,* Mingdong Dai, and David Lee Phillips*

Cite This: https://dx.doi.org/10.1021/acs.joc.0c01115 Read Online

ABSTRACT: In this work, 2,4′-dichlorobiphenyl (**1**) yielded 4′-chloro-2-hydroxybiphenyl (**2**) after photolysis in neutral acetonitrile aqueous (ACN−H_2O) solutions. Ultrafast spectroscopic measurements and density functional theory (DFT) computations were performed for **2** in ACN and ACN−H_2O (v/v, 1:1). These results were compared with previously published results for 2-hydroxybiphenyl (**3**). The counterparts **2** and **3** went through a singlet excited state intramolecular proton transfer (ESIPT) in ACN but behaved differently in ACN−H_2O with a dehydrochlorination process occurring for **2** and an ESIPT taking place for **3**. Computational results indicate that the phenol O−H bond elongates after photoexcitation to induce a concerted asynchronous process with the C−Cl bond increasing first followed by HCl elimination. A biradical intermediate (IM1) is then formed with some spin located at the phenyl 4′-C radical that appears to favor a hydrogen atom transfer (HAT) process and some spin located on phenoxyl that appears to prefer a subsequent •CH_2CN radical rebound. The hydrogen bond promotes HCl elimination, while this is disfavored for ESIPT, making 4′-Cl extrusion the predominant process in ACN−H_2O solutions. The mechanistic investigations have fundamental and significant implications for the understanding of polychlorinated biphenyl photolysis in an aqueous environment and hence the photodegradation of these kinds of pollutants in the natural environment.

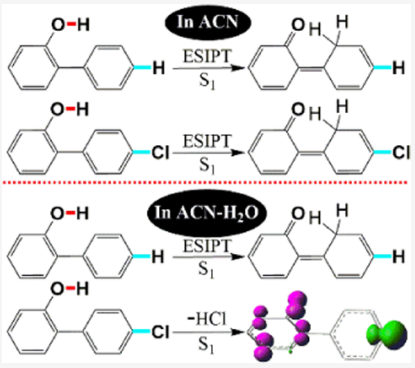

■ INTRODUCTION

Polychlorinated biphenyls (PCBs) are prevalent in the natural environment. Due to their tendency to bioaccumulate and act as a carcinogen,[1] much research has been done on the PCBs' photochemical fate in the environment and in laboratory settings.[2−5] The photolyzed PCBs may dechlorinate in the presence of water, yielding less chlorinated congeners such as chloro-hydroxybiphenyl.[6,7] The PCB photoproducts are also environmental contaminants themselves and this indicates the necessity for investigating their photochemical behavior so as to gain a more complete picture of the fate of the PCB class of chemicals in the environment.

In particular, previous research has indicated that *o*-phenylphenol is a chemical capable of cytotoxic effects to living organisms.[8] Dulin and co-workers[6] reported that 2-chlorobiphenyl yields an acetonitrile (ACN) adduct product 2-acetamidebiphenyl via nucleophilic addition after being photolyzed in neutral ACN aqueous (ACN−H_2O) solutions. A mechanistic investigation on the analog 4-chorobiphenyl thus has new importance.

For simplicity, 2,4′-dichlorobiphenyl (**1**) was chosen as the starting PCB in this contribution as its *ortho*-substitution has been shown to increase its photoreactivity.[2,9,10] Here, we attempt to clarify how the acetonitrile adduct product is formed via a photolysis of 4′-chloro-2-hydroxybiphenyl (**2**) in the presence of water. Gas chromatography−mass spectrometry (GC/MS), femtosecond transient absorption (fs-TA), nanosecond transient absorption (ns-TA), and density functional theory (DFT) calculations were all conducted to study the photolysis of **2** in ACN and ACN−H_2O, respectively. These new results were then compared with previously published results on the related analog 2-hydroxybiphenyl (**3**). The main finding is that a dehydrochlorination intermediate promotes a HAT process followed by a radical rebound to accomplish the ACN adduct formation after photolysis of **2** in the presence of water.

■ RESULTS AND DISCUSSION

GC/MS Results. Compound **2** (yield: ∼10%) and 2-acetamide-4′-chlorobiphenyl (**4**, yield: ∼90%) were produced after photolysis of **1** in ACN−H_2O as determined by GC/MS (Scheme 1, eq 1). The *ortho*-Cl is, respectively, substituted by an OH group and acetamide group, which is consistent with the case for 2-chlorobiphenyl (**5**) (Scheme 1, eq 2) reported by Dulin and co-workers.[6] The 4-Cl seems less reactive than 2-Cl so that the *para* dechlorinated product is not detected for **1** (Scheme 1, eq 1) and 2-methoxy-4′-chlorobiphenyl (**7**) (Scheme 1, eq 3) in ACN−H_2O.

Received: May 8, 2020
Published: August 26, 2020

Scheme 1. Reactions Discussed in the Present Article

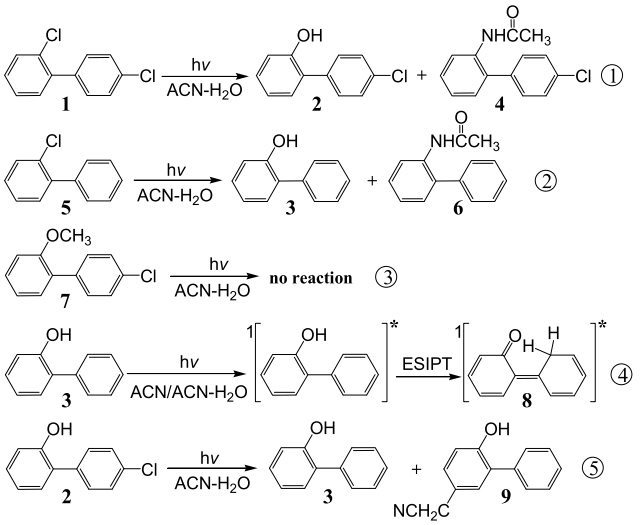

On the above basis, we examined the photochemical activities of the photolysis product of **2**, another 4-Cl compound which is expected to behave similar to **3**. Previous studies reported an excited state intramolecular proton transfer (ESIPT) reaction (Scheme 1, eq 4) for the photolysis of **3** in ACN as well as in ACN−H_2O solutions.[11,12] Steady-state photolysis experiments were performed for **2** in ACN−H_2O (v/v, 1:1). Unexpectedly, there were two main kinds of photoproducts, **3** and the ACN adduct product **9** (Scheme 1, eq 5), which involves a para dechlorination, and the latter was determined to be the primary photoproduct using the GC/MS test (see Figure 1). For the ortho compounds **1** and **5** in

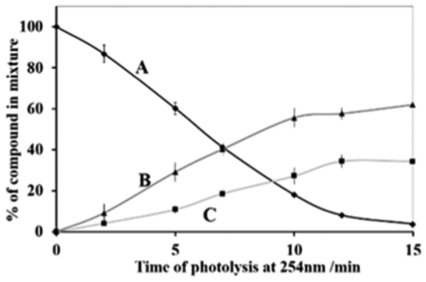

Figure 1. (A) Decomposition of **2** and growth of (B) **9** and (C) **3** after the photolysis of **2** in ACN−H_2O (v/v, 1:1) as measured by GC/MS.

ACN−H_2O solutions, ACN adducts were also the primary photoproducts. These unexpected results indicate that even though H_2O is a better nucleophile, ACN is added preferentially in these systems.

It should be noted that the dechlorination and ACN adduct processes display significant differences between 2-Cl and 4-Cl, in which the 2-Cl system is substituted by OH or the acetamide group, while in the 4-Cl system the Cl is replaced by either a H atom or ACN is not added on the *para*-C atom. Nucleophilic addition is proposed as the dechlorination process for the *ortho*-substitution.[6] However, the above experimental observations suggest that there might be some other reaction pathway responsible for the ACN adduct after photolysis of **2**.

fs-TA and ns-TA Study of 2. fs-TA and ns-TA experiments were first conducted for **2** in ACN and these results were found to be similar to those for **3** in ACN.[13] The first species has a strong absorption at 415 nm with a tail from 550 to 700 nm (Figure 2a) is assigned to ^{1}**2** (left superscript 1

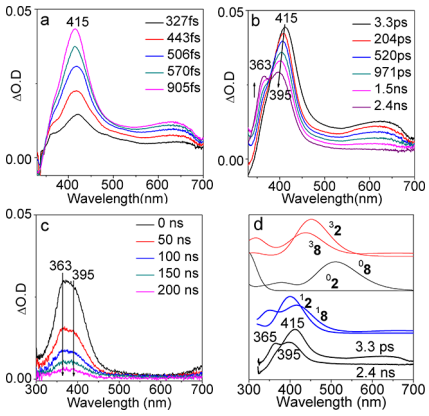

Figure 2. fs-TA and ns-TA obtained for **2** in ACN under the excitation of 266 nm and TD-M062X/6-311g**/SMD (ACN) results with a scale factor of 1.2 (left superscript numbers 0, 1, and 3 indicate the ground state, lowest singlet excited state, and triplet state, respectively).

indicates the lowest singlet excited state), which then converts to a new species that has shoulder bands at 363 and 395 nm (see Figure 2b) and decays from 2.4 to 200 ns (see Figure 2c). With the help of time-dependent (TD-DFT) calculations (Figure 2d) this new species can be attributed to a singlet ESIPT product (also denoted as ^{1}**8** though it has the 4′-Cl group) formed from a phenol proton transfer to an adjacent aromatic *ortho*-C atom. The similar time-resolved spectroscopic results for **2** in MeOH (Figures 2S−5S) suggested that ESIPT is also the predominant process in this H-bonding solvent.

The fs-TA and ns-TA data for **2** in neutral ACN−H_2O (v/v, 1:1) solutions (Figure 3) are significantly different from those observed in ACN for **2** and that in ACN−H_2O (v/v, 1:1) for **3** (see published results[11−13]). Accompanying the generation of ^{1}**2** (at 415 nm), a new species with a broad absorption in the region of 450−700 nm was observed (Figure 3a). This new

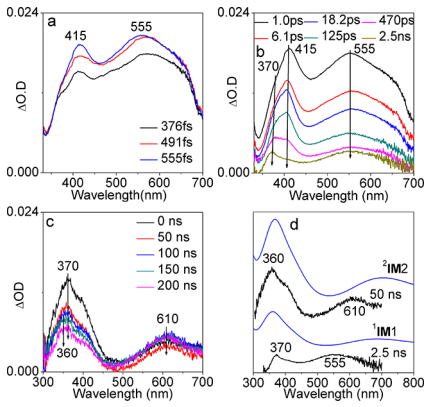

Figure 3. fs-TA and ns-TA spectra of **2** in ACN−H_2O (v/v, 1:1) under the excitation of 266 nm and TD-M062X/6-311g**/SMD (ACN) results with a scale factor of 1.2 (left superscript numbers 1 and 2, respectively, mean an open-shell singlet state and radical).

https://dx.doi.org/10.1021/acs.joc.0c01115
J. Org. Chem. XXXX, XXX, XXX−XXX

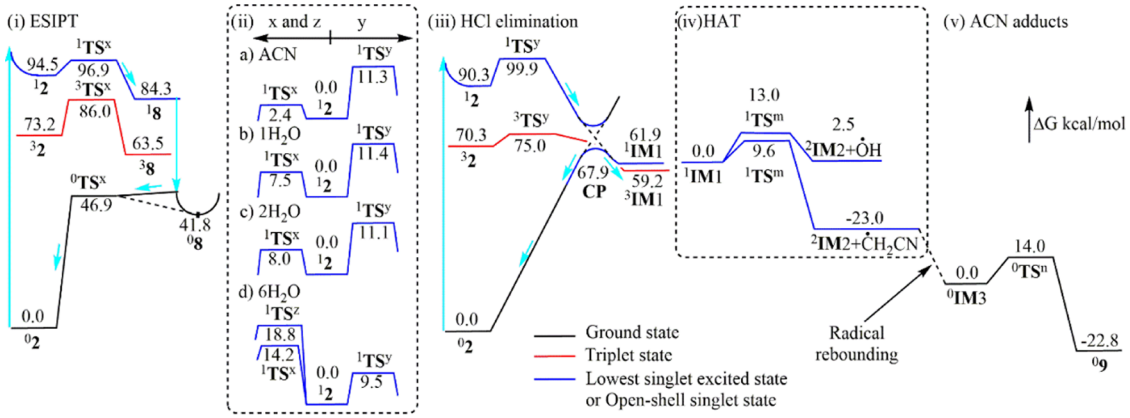

Figure 4. Potential energy surface profiles of **2** in ACN and ACN−H_2O solution were mapped employing (TD)M062X/6-311G**/SMD(ACN) calculations. Paths x, y, z, m, and n on the right superscript represent ESIPT, HCl elimination, ESPT, HAT, and ACN adducts, respectively.

signal is tentatively assigned to be the solvated electrons based on similarity to some literature results.[14] Both ^{1}**2** and the solvated electrons decayed after 1.0 ps and a new transient intermediate (denoted as **IM1**) appeared at 370 and 555 nm, which was observable during the time region of 18.2 ps to 2.5 ns (Figure 3b). The ns-TA for **2** detected **IM1** (370 and 555 nm) mixed with a new transient intermediate species (denoted as **IM2**) with absorption features at 360 and 610 nm (Figure 3c). The absorption bands for **IM1** were quenched from 18.2 ps to 50 ns. **IM2** is a relatively long-lived species (at least 200 ns). Since PCBs tend to dechlorinate **IM1** after photoexcitation, the experimental spectra of **IM1** and **IM2** were, respectively, compared with the simulated electronic absorption spectra of several probable intermediates related with the dechlorination process. It was found that **IM1** exhibited a reasonable similarity with the calculated ultraviolet−visible (UV−vis) spectrum of ^{1}**IM1** or ^{3}**IM1** (left superscript 3 indicates the triplet state, Figures 3d and 8S). ^{1}**IM1** was located using a broken symmetry methodology but not via the TD-DFT method. ^{1}**IM1** and ^{3}**IM1** have a biradical character formed via a HCl elimination process. This attribution is in agreement with the fact that the absorption bands at 370 and 555 ns were quenched when oxygen is present in the solution. The **IM2** signal at 50 ns is similar to that in the calculated UV−vis spectrum (see Figure 3d) for ^{2}**IM2** (left superscript 2 indicates radical species), which has a phenoxy radical character and can be produced by a HAT to ^{1}**IM1**. This assignment is consistent with the experimental result that **IM2** is not affected by the presence or absence of oxygen in the solution.

DFT Study of 2. To investigate the mechanism in detail, the potential energy surface profiles of **2** in ACN (Figure 4i) were studied. The electronic transition from ^{0}**2** (left superscript 0 means the ground state S_0) to ^{1}**2** was induced upon irradiation (Figure 4a). ^{1}**2** overcomes an energy barrier of 2.4 kcal/mol and then the transition state ^{1}**TS**^{x} (right superscript x means ESIPT) goes downhill to ^{1}**8** by an exothermic process (12.6 kcal/mol). ^{1}**8** is a long-lived species (at least 200 ns) and decays by the internal conversion (IC) to a highly vibrational state of ^{0}**8**, which is unstable and soon goes through ^{0}**TS**^{x} via a barrierless pathway to the starting material ^{0}**2** (Figure 6S).The photochemical process induced by ^{3}**2** seems difficult because of the fast singlet ESIPT process.

The dechlorination process on the S_1 surface in ACN can be ruled out as ^{1}**TS**^{y} (right superscript y means dechlorination) is 8.9 kcal/mol higher in energy than ^{1}**TS**^{x} (Figure 4iia). TD-DFT calculations were performed for **2** with $1H_2O$ and $2H_2O$ added explicitly to the reaction system, respectively (Figure 4iib,c) and ESIPT is still more favored than the dechlorination with energy gap differences of 3.9 and 3.1 kcal/mol for $1H_2O$ and $2H_2O$ cases, respectively. However, when $6H_2O$ was added explicitly in the reaction system, dechlorination becomes the preferential process with a 3.7 kcal/mol lower in energy barrier than ESIPT (see Figure 4iid).

The potential energy surface profile for **2** with $6H_2O$ (see Figure 4iii) shows that an S_1 surface starting from ^{1}**2** goes through ^{1}**TS**^{y} with an activation energy of 9.6 kcal/mol. Photoexcitation occurs mainly on the aromatic π electrons of ^{1}**2** (see Figure 5), which should have little effect on the in-

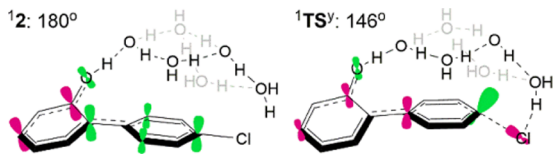

Figure 5. Angle between the C−Cl bond and the adjacent phenyl ring and the spin distribution for ^{1}**2** and ^{1}**TS**^{y} with $6H_2O$. (Unit: °).

plane C−Cl σ bond. However, the angle between the C−Cl bond and the adjacent phenyl ring decreased from 180° in ^{1}**2** to 146° in ^{1}**TS**^{y} (see Figure 5), and the excited π electrons can gain a conjugation interaction with the C−Cl σ bond to facilitate the Cl anion extrusion. The charge is transferred from the electron-donor phenol to the electron-acceptor chlorophenyl, which is favored for the deprotonation and the system then dechlorinates,[15−17] and this can be further promoted by the intermolecular H-bonding between the phenol O−H bond and the H_2O molecules. The triplet species ^{3}**2** is not considered because of the big energy gap (20.0 kcal/mol) with ^{1}**2** makes the intersystem crossing (ISC) less efficient than the singlet excited state dechlorination process. The IRC calculation reveals that ^{1}**TS**^{y} will go forward to a conical point (denoted as **CP**) between the S_1 and S_0 surfaces before it reaches the dehydrochlorination intermediate ^{1}**IM1**. This **CP** can be located using the broken symmetry methodology, which is an open-shell singlet TS. This **CP** can go backward to ^{0}**2** ($\langle S^2 \rangle = 0$ as seen in the IRC calculation results), while it will go forward to the dehydrochlorination intermediate ^{1}**IM1** ($\langle S^2 \rangle = 1.0387$ as seen in the IRC calculation results). This can

https://dx.doi.org/10.1021/acs.joc.0c01115
J. Org. Chem. XXXX, XXX, XXX−XXX

be supported by the fact as shown in Figure 3b and 4iii that ^{1}**2** decays much faster than ^{1}**IM1** formation, intimating that ^{1}**2** went through the **CP** and then mainly went back to the starting material ^{0}**2**, while only a little amount produces ^{1}**IM1**. After ^{3}**TS**^{y}, the triplet surface also goes close to the **CP** so that ^{3}**IM1** is mixed with ^{1}**IM1** (Figures 7S and 8S) and ^{1}**IM1** is employed to do the DFT calculations in consideration of the subsequent radical rebound. ^{1}**IM1** has a biradical character with one phenoxyl α spin and one phenyl β radical (see Scheme 2).

Scheme 2. Proposed ACN Adduct Formation Mechanism of 2 in ACN−H_2O Solution[a]

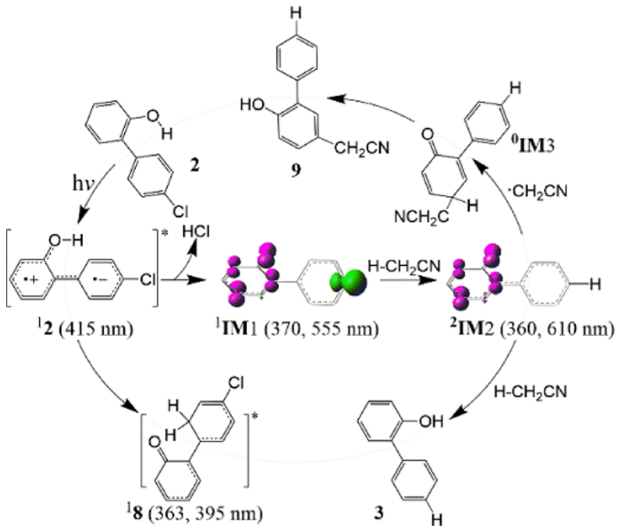

[a]The spin population for key intermediates ^{1}**IM1** and ^{2}**IM2** are indicated (isovalue: 0.014).

^{1}**IM1** performs as the precursor for the following reaction. The phenyl 4′-C radical is reactive for HAT from ACN, a better H-donor with a lower energy barrier of 9.6 kcal/mol leading to a larger exothermic process of 23.0 kcal/mol than the case for H_2O (Figure 4iv). Then, ^{2}**IM2** is formed with one spin mainly delocalized to the phenoxy O and 5-C atoms (see Scheme 2). It should be noted that ^{2}**IM2** also might be produced by an excited state proton transfer (ESPT) from a phenol proton to the 4′-C atom accompanied with the Cl atom extrusion, while this possibility is ruled out because it has a higher energy barrier of 18.8 kcal/mol compared to that of the HAT pathway (Figure 4iid, ^{1}**TS**^{z}). The phenoxy O and 5-C atoms are two possible active sites for the following •CH_2CN radical rebound. The •CH_2CN radical combined with the 5-C atom produces the ground state intermediate ^{0}**IM3**, which then will go through a TS with an activation energy of 14.0 kcal/mol and an exothermic process of 22.8 kcal/mol to form the ACN adduct **9** (Figure 4v). That is, it is not a nucleophilic addition but is a dehydrochlorination intermediate promoted HAT followed by a radical rebound for the inert ACN to be added onto **2** (Scheme 2).

The O−H and C−Cl bond distances for ^{1}**2** and ^{1}**TS**^{y} with ACN, 1H_2O, 2H_2O, and 6H_2O are listed in Figure 6. The O−H bond is elongated from 0.97 to 1.06 Å, while the C−Cl bond changed little at 1.74−1.75 Å for ^{1}**2** as the number of H_2O increased, corresponding to the H-bonding between the phenol O−H bond and H_2O increasing with the number of water molecules in the system and ESIPT requires extra energy to break the strong H-bonding in ACN−H_2O so that the ESIPT energy barrier for **2** in 6H_2O (14.2 kcal/mol) is much higher than that in ACN (2.4 kcal/mol, Figure 4ii); and therefore opens a door for the dehydrochlorination in ACN−H_2O. Furthermore, the elongated phenol O−H bond promotes charge transfer and earns power to favor the following Cl extrusion via the π−σ conjugation in ^{1}**TS**^{y} with 6H_2O (see Figure 5), decreasing the dehydrochlorination energy barrier for **2** (9.5 kcal/mol) (Figure 4ii). This is supported by the fact that ^{1}**TS**^{y} just has the Cl extrusion character since the phenol O−H bond changed little compared to that on ^{1}**2** (see Figure 6). Intrinsic reaction coordinate (IRC) calculations revealed that both O−H and C−Cl bonds are elongated after ^{1}**TS**^{y} in the 6H_2O case. Therefore, the phenol O−H bond elongated by H-bonding after photo-excitation induces a concerted asynchronous HCl elimination.

ESIPT is not considered for methoxy-substituted biphenyl (**7**). The dechlorination energy barrier for **7** in ACN−H_2O should be similar to that (∼11.3 kcal/mol) for **2** in ACN (see Figure 4iia). However, **7** is found to be photostable (Scheme 1, eq 5), intimating that HCl elimination is decisive for 4′-Cl extrusion, which is significantly different from the 2-Cl cleavage (Scheme 1, eqs 1 and 2). The dehydrochlorination linked together by a water bridge occurs by a proton transfer from the proton-donating phenol OH group to water. Methanol can also serve as the solvent bridge for the proton transfer, while no MeOH adducts were detected in neat MeOH even in MeOH−H_2O (v/v, 4:1) (Figure 1S-4S). Agmon et al.[18] pointed out that the number of hydrogen bonds, both made and broken, facilitate the proton transfer as well as dielectric stabilization of the anion. The fact that water can donate two hydrogen bonds and methanol only one is critical, in that methanol must break its lone hydrogen bond in order to form

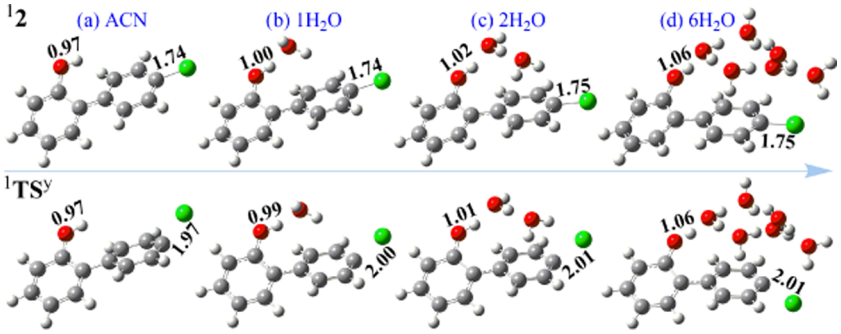

Figure 6. Phenol O−H and C−Cl bond distances of ^{1}**2** and ^{1}**TS**^{y} with ACN, 1H_2O, 2H_2O, and 6H_2O (unit: Å).

https://dx.doi.org/10.1021/acs.joc.0c01115
J. Org. Chem. XXXX, XXX, XXX−XXX

a new one. This distinction is subtle but has an important impact on the kinetics, which was further supported by the high-level calculations by Hynes et al. to predict the trajectory of proton transfer and the role of solvent reorganization in the reaction coordinate.[19] Therefore, the proton transfer occurs with a bigger methanol cluster and increases the entropic requirements (not the enthalpic effect) for the proton transfer compared to the water solvent.[20] Then, less energy is required to break the H-bonding between MeOH and phenol OH and the ESIPT energy barrier is still lower than the dehydrochlorination for **2**. ESIPT then is still favored over the dehydrochlorination and no HCl elimination occurred and no MeOH adducts were observed though MeOH is a better H-donor than ACN.

■ CONCLUSIONS

In summary, the dehydrochlorination is decisive for *para*-Cl dechlorination and the formation of subsequent ACN adducts that is an interesting incorporation of the cosolvent ACN (this is remarkably different from the reactions observed for *ortho*-Cl biphenyls when H_2O is present). This finding is important as it increases the overall understanding of PCB photochemistry, as the chloro-hyroxybiphenyls are an important photochemical product of these PCBs, which also have associated environmental concerns. By changing the substitution pattern of the biphenyls, different patterns of reactivity are envisaged. These results may open up another series of compounds that react via dechlorination intermediates that are relevant in environmental photochemistry and also promising in synthetic chemistry. This preference for incorporation of the solvent (in this case ACN) is due to the H-donor ability of these compounds. Perhaps they will also react with other better H-donor organic compounds in the aqueous environment and find a wider use in chemistry.

■ EXPERIMENTAL AND COMPUTATIONAL METHODS

Compounds **1** and **2** were synthesized by utilizing previously reported methods detailed in the literature[21,22] and the synthesis routes are shown in Schemes 1S and 2S, respectively. For characterization of the samples prepared, please see the NMR (^{1}H, ^{13}C) spectra displayed in the Supporting Information.

All photolysis experiments were conducted in a Rayonet RPR 100 containing 16 lamps (350 nm). Cooling was achieved with an internal cold finger. The sample solutions (3×10^{-3} M) were prepared in ACN−H_2O and purged with argon 15 min prior to irradiation. Following photolysis, the solutions were extracted with CH_2Cl_2 and dried over $MgSO_4$. All photoproducts were isolated by preparative thin-layer chromatography (PTLC) in ethyl acetate/hexane and identified by NMR (^{1}H, ^{13}C) and MS.

Photoproduct 4′-chloro-2-hydroxybiphenyl (**2**), a pale yellow oil, was isolated from the photolysis mixture of **1** in 1:1 ACN−H_2O by PTLC (silica gel, 1:5 ethyl acetate/hexane) and confirmed by MS with M^+ at 204, ^{1}H NMR (400 MHz, $CDCl_3$/TMS) δ (ppm): 5.27 (s, 1H), 6.97 (dd, J = 8.1, 1.0 Hz, 1H), 7.03 (td, J = 7.5, 1.1 Hz, 1H), 7.24−7.31 (m, 2H), 7.42−7.49 (m, 4H) and ^{13}C{1H} NMR (100 MHz, $CDCl_3$/TMS) δ (ppm): 116.2, 121.2, 127.2, 129.3, 129.5, 130.4, 130.6, 133.8, 135.8, 52.4.

Photoproduct 2-acetamide-4′chlorobiphenyl (**4**), a pale yellow solid, was isolated from the photolysis mixture of **1** in 1:1 ACN−H_2O by PTLC (silica gel, 1:5 ethyl acetate/hexane) and confirmed by MS with M^+ at 245 and ^{1}H NMR (400 MHz, $CDCl_3$/TMS) δ (ppm): 2.03 (s, 3H), 7.05 (s, 1H), 7.20 (t, J = 7.2 Hz, 2H), 7.27−7.33 (m, 2H), 7.34−7.40 (m, 1H), 7.45 (d, J = 8.4 Hz, 2H), 8.16 (d, J = 8.2 Hz, 1H).

The ACN adduct **9**, a pale yellow oil, was isolated from the photolysis mixture of **2** by PTLC (silica gel, 1:2 ethyl acetate/hexane) and characterized by MS, HRMS, ^{1}H NMR, ^{13}C{1H} NMR, long-range heteronuclear correlation (HETCOR), and COSY. ^{1}H NMR (400 MHz, $CDCl_3$/TMS) δ (ppm): 3.71 (s, 2H), 5.42 (s, 1H), 6.95−7.02 (m, 1H), 7.17−7.23 (m, 2H), 7.41−7.53 (m, 5H). ^{13}C{1H} NMR ($CDCl_3$) δ (ppm): 152.5 (C−OH), 118.0, 136.4 (11C), 116.8 (1C, ortho to CH_2CN and the adjacent phenyl ring), 23.09 (−CH_2−). Long-range HETCOR confirmed that the hydroxyl group is para to the CH_2CN group, with ^{1}H COSY further confirming that these substituents are on the same ring. MS 209 m/z (M^+). HRMS calcd for $C_{14}H_{11}NO$ 209.0790, found 209.0796. HRMS calcd for $C_{14}H_{10}NO$ (M−H) 208.0757, found 208.0770. Other minor ACN adducts were formed only in trace yields and could not be identified with confidence.

The fs-TA experiments were done employing a commercial regenerative amplified Ti/sapphire laser system and similarly, the ns-TA experiments were done using a commercial laser flash photolysis apparatus. The fs-TA experiments used 267 nm photolysis and a white light continuum (330−800 nm) probe laser pulse while the ns-TA experiments utilized 266 nm laser photoexcitation and a xenon lamp for the probe light. An absorbance of unity at 266 nm was used for the sample solutions in the fs-TA and ns-TA experiments. More details of the fs-TA and ns-TA tests are described elsewhere.[23]

The DFT computations employed the (U)M062X/6-311G**/SMD(ACN) level of theory to find the optimized geometries and vibrational wavenumbers for the transients considered to be possible intermediates for the reactions of interest in this study. All of the calculations used the Gaussian 16 program suite.[24] Further details of the calculations are given in the Supporting Information.

■ ASSOCIATED CONTENT

Supporting Information

The Supporting Information is available free of charge at https://pubs.acs.org/doi/10.1021/acs.joc.0c01115.

fs-TA spectra of the reported species, optimized geometries of the RC, TS, and PC, the reaction energy profile obtained from the M062X/6-311G** calculations, and the excited state energies and oscillator strengths from the TD-DFT (M062X/6-311G**) calculations for the transient species along with the Cartesian coordinates, Gibbs free energies, and the thermal correction to the Gibbs free energy for the optimized geometry from the M062X/6-311G** calculations for the compounds and intermediates (PDF)/.

■ AUTHOR INFORMATION

Corresponding Authors

Jiani Ma − *Key Laboratory of Synthetic and Natural Functional Molecule Chemistry of Ministry of Education, College of Chemistry and Materials Science, Northwest University, Xi'an 710172, P. R. China;* orcid.org/0000-0003-3325-0762; Email: majiani@nwu.edu.cn

David Lee Phillips − *Department of Chemistry, The University of Hong Kong, Hong Kong 999077, P. R. China;* orcid.org/0000-0002-8606-8780; Email: phillips@hku.hk

Authors

Xiting Zhang − *Key Laboratory of Synthetic and Natural Functional Molecule Chemistry of Ministry of Education, College of Chemistry and Materials Science, Northwest University, Xi'an 710172, P. R. China; Department of Chemistry, The University of Hong Kong, Hong Kong 999077, P. R. China;* orcid.org/0000-0001-7602-1965

https://dx.doi.org/10.1021/acs.joc.0c01115
J. Org. Chem. XXXX, XXX, XXX−XXX

Yan Guo − *Key Laboratory of Synthetic and Natural Functional Molecule Chemistry of Ministry of Education, College of Chemistry and Materials Science, Northwest University, Xi'an 710172, P. R. China*

Erin Dallin − *Department of Chemistry, University of Victoria, Victoria, British Columbia V8W 2Y2, Canada*

Mingdong Dai − *Key Laboratory of Synthetic and Natural Functional Molecule Chemistry of Ministry of Education, College of Chemistry and Materials Science, Northwest University, Xi'an 710172, P. R. China*

Complete contact information is available at: https://pubs.acs.org/10.1021/acs.joc.0c01115

Author Contributions

X.Z. and Y.G. contributed equally. The manuscript was written through contributions of all authors and all have given approval to the final version of the manuscript.

Notes

The authors declare no competing financial interest.

■ ACKNOWLEDGMENTS

The research was sponsored in part by grants from the National Natural Science Foundation of China (21973075) to J.M. and the Research Grants Council of Hong Kong (HKU17301815) to D.L.P. and partial support from the Areas of Excellence Scheme (Grant AoE/P-03/08), the UGC Special Equipment Grant (SEG-HKU-7), and the University of Hong Kong Development Fund 2013-2014 project "New Ultrafast Spectroscopy Experiments for Shared Facilities". We would like to thank Peter Wan for useful discussion of this work.

■ REFERENCES

(1) Baxter, R. M.; Sutherland, D. A. Biochemical and Photochemical Processes in the Degradation of Chlorinated Biphenyls. *Environ. Sci. Technol.* **1984**, *18*, 608−610.

(2) Ruzo, L. O.; Zabik, M. J.; Schuetz, R. D. Photochemistry of Bioactive Compounds. Photochemical Processes of Polychlorinated Biphenyls. *J. Am. Chem. Soc.* **1974**, *96*, 3809−3813.

(3) Matykiewiczová, N.; Klánová, J.; Klán, P. Photochemical Degradation of PCBs in Snow. *Environ. Sci. Technol.* **2007**, *41*, 8308−8314.

(4) Lepine, F. L.; Milot, S. M.; Vincent, N. M.; Gravel, D. Photochemistry of Higher Chlorinated PCBs in Cyclohexane. *J. Agric. Food Chem.* **1991**, *39*, 2053−2056.

(5) Chu, W.; Chan, K. H.; Kwan, C. Y.; Jafvert, C. T. Acceleration and Quenching of the Photolysis of PCB in the Presence of Surfactant and Humic Materials. *Environ. Sci. Technol.* **2005**, *39*, 9211−9216.

(6) Dulin, D.; Drossman, H.; Mill, T. Products and Quantum Yields for Photolysis of Chloroaromatics in Water. *Environ. Sci. Technol.* **1986**, *20*, 72−77.

(7) Bunce, N. J. Photolysis of 2-Chlorobiphenyl in Aqueous Acetonitrile. *Chemosphere* **1978**, *7*, 653−656.

(8) Nakagawa, Y.; Tayama, S.; Moore, G.; Moldéus, P. Cytotoxic Effects of Biphenyl and Hydroxybiphenyls on Isolated Rat Hepatocytes. *Biochem. Pharmacol.* **1993**, *45*, 1959−1965.

(9) Scheve, B. J.; Wagner, P. Triplet State Geometries of Methyl-Substituted Biphenyls. *Chem. Phys. Lett.* **1974**, *25*, 324−327.

(10) Bunce, N. J. Photodechlorination of PCB's: Current Status. *Chemosphere* **1982**, *11*, 701−714.

(11) Lukeman, M.; Wan, P. Excited State Intramolecular Proton Transfer (ESIPT) in 2-Phenylphenol: an Example of Proton Transfer to a Carbon of an Aromatic Ring. *Chem. Commun.* **2001**, 1004−1005.

(12) Lukeman, M.; Wan, P. A New Type of Excited-State Intramolecular Proton Transfer: Proton Transfer from Phenol OH to a Carbon Atom of an Aromatic Ring Observed for 2-Phenylphenol. *J. Am. Chem. Soc.* **2002**, *124*, 9458−9464.

(13) Ma, J.; Zhang, X.; Basarić, N.; Wan, P.; Phillips, D. L. Observation of Excited State Proton Transfer Reactions in 2-Phenylphenol and 2-Phenyl-1-Naphthol and Formation of Quinone Methide Species. *Phys. Chem. Chem. Phys.* **2015**, *17*, 9205−9211.

(14) Kimura, Y.; Alfano, J. C.; Walhout, P. K.; Barbara, P. F. Ultrafast Transient Absorption Spectroscopy of the Solvated Electron in Water. *J. Phys. Chem. A.* **1994**, *98*, 3450−3458.

(15) Lukeman, M.; Wan, P. A New Type of Excited-State Intramolecular Proton Transfer: Proton Transfer from Phenol OH to a Carbon Atom of an Aromatic Ring Observed for 2-Phenylphenol[1]. *J. Am. Chem. Soc.* **2002**, *124*, 9458−9464.

(16) Brousmiche, D. W.; Xu, M.; Lukeman, M.; Wan, P. Photohydration and Photosolvolysis of Biphenyl Alkenes and Alcohols via Biphenyl Quinone Methide-type Intermediates and Diarylmethyl Carbocations. *J. Am. Chem. Soc.* **2003**, *125*, 12961−12970.

(17) Flegel, M.; Lukeman, M.; Huck, L.; Wan, P. Photoaddition of Water and Alcohols to the Anthracene Moiety of 9-(2′-Hydroxyphenyl)anthracene via Formal Excited State Intramolecular Proton Transfer. *J. Am. Chem. Soc.* **2004**, *126*, 7890−7897.

(18) (a) Agmon, N.; Huppert, D.; Masad, A.; Pines, E. Excited-State Proton Transfer to Methanol-Water Mixtures. *J. Phys. Chem. B.* **1991**, *95*, 10407−10413;(b) Excited-state proton transfer to methanol-water mixtures [Erratum to document cited in CA115(25):279306r]. *J. Phys. Chem. C.* **1992**, *96*, 2020.

(19) Andot, K.; Hynes, J. T. HCl Acid Ionization in Waters-A Theoretical Molecular Modeling. *J. Mol. Liq.* **1995**, *64*, 25−37.

(20) Tolbert, L. M.; Solntsev, K. M. Excited-state proton transfer: From constrained systems to "super" photoacids to superfast proton transfer. *Acc. Chem. Res.* **2002**, *35*, 19−27.

(21) Karanjit, S.; Jinasan, A.; Samsook, E.; Dhital, R. N.; Motomiya, K.; Sato, Y.; Tohjic, K.; Sakurai, H. Significant Stabilization of Palladium by Gold in the Bimetallic Nanocatalyst Leading to an Enhanced Activity in the Hydrodechlorination of Aryl Chlorides. *Chem. Commun.* **2015**, *51*, 12724−12727.

(22) Inamoto, K.; Kadokawa, J.; Kondo, Y. Ruthenium-Catalyzed Carbonylative C−H Cyclization of 2-Arylphenols: A Novel Synthetic Route to 6*H*-Dibenzo[*b*,*d*]pyran-6-ones. *Org. Lett.* **2013**, *15*, 3962−3965.

(23) Ma, J.; Zhang, X.; Phillips, D. L. Time-resolved Spectroscopic Observation and Characterization of Water-Assisted Photoredox Reactions of Selected Aromatic Carbonyl Compounds. *Acc. Chem. Res.* **2019**, *52*, 726−737.

(24) Frisch, M. J.; Trucks, G. W.; Schlegel, H. B.; Scuseria, G. E.; Robb, M. A.; Cheeseman, J. R.; Scalmani, G.; Barone, V.; Petersson, G. A.; Nakatsuji, H.; Li, X.; Caricato, M.; Marenich, A. V.; Bloino, J.; Janesko, B. G.; Gomperts, R.; Mennucci, B.; Hratchian, H. P.; Ortiz, J. V.; Izmaylov, A. F.; Sonnenberg, J. L.; Williams-Young, D.; Ding, F.; Lipparini, F.; Egidi, F.; Goings, J.; Peng, B.; Petrone, A.; Henderson, T.; Ranasinghe, D.; Zakrzewski, V. G.; Gao, J.; Rega, N.; Zheng, G.; Liang, W.; Hada, M.; Ehara, M.; Toyota, K.; Fukuda, R.; Hasegawa, J.; Ishida, M.; Nakajima, T.; Honda, Y.; Kitao, O.; Nakai, H.; Vreven, T.; Throssell, K.; Montgomery, J. A., Jr.; Peralta, J. E.; Ogliaro, F.; Bearpark, M. J.; Heyd, J. J.; Brothers, E. N.; Kudin, K. N.; Staroverov, V. N.; Keith, T. A.; Kobayashi, R.; Normand, J.; Raghavachari, K.; Rendell, A. P.; Burant, J. C.; Iyengar, S. S.; Tomasi, J.; Cossi, M.; Millam, J. M.; Klene, M.; Adamo, C.; Cammi, R.; Ochterski, J. W.; Martin, R. L.; Morokuma, K.; Farkas, O.; Foresman, J. B.; Fox, D. J. *Gaussian 16*, revision A.03; Gaussian, Inc.: Wallingford, CT, 2016.